ORIGINAL PAPER

Au/CeO$_2$ metallic monolith catalysts: influence of the metallic substrate

L. M. Martínez Tejada · M. I. Domínguez · O. Sanz ·
M. A. Centeno · J. A. Odriozola

Abstract Ceria-based gold catalysts were successfully deposited on ferritic stainless steel (Fecralloy) and aluminium monoliths. The prepared monolithic and reference powder catalysts were characterized by means of S_{BET}, X-ray diffraction, glow discharge optical emission spectroscopy and scanning electron microscopy–energy dispersive X-ray analysis techniques and tested in the CO oxidation reaction. Characterization results put in evidence the diffusion of cations from the catalytic layer on the surface of the monoliths to the metallic oxide scale and inversely, from the oxide scale to the catalysts, thus altering the catalytic formulation and affecting the CO oxidation properties of the catalytic device. The extension and nature of the modifications produced depend on the nature of the catalysts and the metallic substrate, as well as the reaction conditions applied. These facts must be considered when gold catalysts are supported on metallic-structured devices.

Introduction

Heat and mass transport properties are strongly enhanced by using structured catalysts and reactors that offer high precision in catalysis at all relevant scales of the catalytic processes. Monoliths of longitudinal parallel channels, an example of

L. M. Martínez Tejada (✉) · M. I. Domínguez · O. Sanz ·
M. A. Centeno · J. A. Odriozola
Departamento de Química Inorgánica—Instituto de Ciencia de
Materiales de Sevilla, Centro Mixto Universidad de Sevilla-CSIC,
Avda. Américo Vespucio 49, 41092 Sevilla, Spain
e-mail: leidy@icmse.csic.es

such catalytic devices, have wide practical applications, especially in environmental applications [1], resulting in a valuable alternative to conventional fixed beds, for instance due to their low-pressure drop at high flow rates. Monoliths can be made of ceramic or metallic materials. Metallic monoliths show some advantages over ceramic ones such as higher thermal conductivity, lower heat capacities and greater thermal and mechanical shock resistance [2]. These advantages make them the best option for catalytic reactions in which the control of the reaction heat and temperature is a key issue. However, the adherence of the catalysts to the metallic substrate still remains a problem.

The most popular method to coat monolithic structures is washcoating. For this method, a homogeneous and stable colloidal suspension of the catalyst with the adequate rheological and compositional properties (solids content and particle size, pH, viscosity, addition of surfactants and stabiliser, etc.) must be carefully prepared in order to successfully achieve a uniform deposition of the catalyst on the metallic surface [3]. Besides this, a suitable pre-treatment of the metallic substrate is also necessary to favour the adhesion. The most popular pre-treatments consist of generating a stable, resistant, rough, well-adhered and homogenous oxide scale on the surface, directly grew from the metallic bulk. The composition of such oxide scale, as well as the pre-treatment method used, depends on the metal substrate [4, 5]. Thus, thermal treatments have been demonstrated as very efficient for austenitic [3, 6, 7] and ferritic stainless steels [7–9] while anodisation is the elected method for aluminium surfaces [10, 11]. Thermal treatment in synthetic air at 900 °C for 1 h of AISI 304 monoliths generates an oxide layer composed mainly of chromium oxide and Mn–Cr–spinel type compounds [12], while thermal treatments at 900 °C for 22 h produces an open structure of long and randomly oriented α-Al$_2$O$_3$ whiskers in ferritic stainless steels containing 3–5 % of Al, as Fecralloy and Aluchrom YHf [7–9]. Finally, anodisation processes induce the formation of a porous amorphous alumina

Springer

layer on the surface of the metallic aluminium [10]. The texture of such alumina coating can be controlled by tuning up the anodisation parameters such as time, current density, temperature, electrolyte nature and its concentration. The anodic films contain fine porosity as perpendicular channels reaching the alumina–aluminium interface, which is formed by a barrier layer that separates the pores from the metallic aluminium. However, when the anodisation conditions are extreme, an important cracking of the surface appears with wide and deep cracks [11].

On the other hand, the relevance and uses of gold catalysts continuously grow from the pioneer works of Haruta and Hutchings [13, 14], as evidenced by the vast number of papers and industrial patents appeared in the last years. The main efforts have been addressed to amplify the use of gold in different catalytic reactions, particularly oxidation ones of interest from the technological and environmental point of view. Thus, the preparation of structured devices incorporating gold catalysts is clearly a challenge topic with interesting foreseeing applications. In this sense, several papers have been published using Au/CeO_2, Au/TiO_2, Au/Fe_2O, Au/KMn_8O_{16}, $Au/CeFe$, $Au/CeCu$, Au/Al_2O_3 and $Au/CuO_x/CeO_2$ [3, 7, 11, 12, 15–22] in oxidation reactions such as preferential (PROX) and total (TOX) oxidation of CO. In most of those works, AISI 304 stainless steel was the selected substrate to prepare the monoliths.

It is well known that the activity and selectivity of gold catalysts depend on gold particle size and morphology, on the nature of the support (redox properties, structure and textural properties) and on the nature of the gold-support interface [23]. From here, it is evident that the success of the preparation of monolithic catalysts with gold passes through the deposition of the catalytic layer with the desired composition and textural, morphological and electronic properties of the gold active phase.

However, we have recently described that after deposition of Au/CeO_2 and CeO_2 catalyst on AISI 304 monoliths, the migration of some elements from the catalytic layer deposited to the oxide scale of the pre-treated metallic substrate and conversely, from the oxide scale to the catalytic layer occurs [12, 22]. This cationic diffusion alters the catalyst formulation and results in the modification of the alloy/oxide scale and oxide scale/coating interfaces, thus affecting the catalytic properties [12]. A similar conclusion was extracted for Au/TiO_2 catalysts deposited on ferritic (Aluchrom YHf) stainless steel monoliths [7].

The aim of this work is to provide evidence that the nature and extension of these modifications depend on both the catalysts formulation and the metallic substrate. For exemplifying, we have selected Au/CeO_2 (0.1 and 1 wt.%) and CeO_2 as catalysts to be deposited on monoliths prepared with two different metallic substrates, a ferritic (Fecralloy) stainless steel and anodised aluminium.

The obtained results are also compared with those previously reported for similar AISI 304 monoliths and powder catalysts [3, 12, 20]. The catalytic implications of the modifications were tested only in the CO oxidation reaction, although the modifications also depends on the catalytic reaction and on the reaction conditions used (atmosphere, temperature, time, etc.). In order to clearly visualize these catalytic implications, a non-conventional method of preparation of gold catalysts was used, which allows obtaining medium size gold particles (from 4 to 20 nm) resulting in no extremely active gold monoliths.

Experimental

Preparation of the structured supports

The composition of the metallic sheets used to prepare the structured supports is shown in Table 1. Ferritic stainless steel (Fecralloy) sheets 50 μm thick were supplied by Goodfellow, and aluminium ones (100 μm thick) by INASA (Industria Navarra de Aluminio S.A). Aluminium sheets were anodised as reported elsewhere [11] (conditions: 2.6 M of sulphuric acid, 30 °C, 50 min and 2 Å dm^{-2}) before conformation of the monolith. The monoliths were manufactured by rolling up corrugated and flat foils around a spindle. The final monoliths are cylinders of 3 cm height, 1.6 cm diameter, 240 cm^2 geometric surface area and a cell density of 55 cell/cm^2. The metallic substrates were pre-treated before anchoring of catalysts. Fecralloy monoliths were thermally treated at 900 °C for 22 h [9, 24] and the anodised aluminium monoliths were calcined at 500 °C for 2 h.

Catalyst coating deposition

A commercial ceria colloid (Nyacol, 20 wt.% CeO_2 with acetate as counter ion) was used for preparing a colloidal solution with 10 wt.% solid content by adding the adequate amount of distilled water. Then, when needed, the adequate

Table 1 Composition of commercial stainless steels

Element (wt%)	Fe	Cr	Si	Al	C	Y	Mn	Mg	Cu	Pb	Ti	Zn
Fecralloy	Balance	22	0.3	4.8	0.003	0.3	–	–	–	–	–	–
Aluminium	0.34	0.0009	0.10	balance	–	–	0.005	0.002	0.002	0.001	0.011	0.05

amount of the metallic gold precursor (gold acetate, Alfa Aesar 99.99 % pure) was added in absence of light [25]. This non-conventional method was selected for its easiness [3, 12, 20], saving the separate gold deposition step on the previous powder ceria and decreasing the preparation time. The use of gold acetate as source of gold instead of the normally used for preparing powder gold catalysts (chloroauric acid) was selected in order to avoid pitting corrosion of the stainless steel surface induced by chlorine ions. Three colloidal solutions were prepared with the adequate composition to prepare monoliths washcoated with CeO_2, $0.1\%Au/CeO_2$ and $1\%Au/CeO_2$ catalysts.

For washcoating, the monoliths were immersed into the adequate colloidal dispersion for 1 min and then withdrawn at $3\ cm\ h^{-1}$. The colloid excess was removed by centrifugation at 400 rpm for 10 min to avoid the obstruction of the channels. After that, the monoliths were dried in an oven. The anodised aluminium monoliths were dried at 60 °C for 1 h to avoid the sealing of alumina pores [11], while 120 °C for 1 h was used for Fecralloy ones [9]. Finally, they were calcined at 300 °C for 4 h with a heating ramp of $2\ °C\ min^{-1}$. Three coating–drying–calcinations stages were necessary to increase the amount of coating until≅100 mg.

Powder Catalysts

Powder catalysts were obtained by drying at 80 °C and further calcination for 4 h at 300 °C of the corresponding colloidal dispersions.

Catalysts characterization

X-ray diffraction (XRD) analysis was performed on a D500 Siemens diffractometer. Diffraction patterns were recorded using Cu-Kα radiation (λ=1.5404 Å) over a 20–80° 2θ range and a position-sensitive detector with 0.05° step size at a scan rate of $1°\ min^{-1}$.

The textural properties were studied by N_2 adsorption–desorption measurements at liquid nitrogen temperature in a Micromeritics ASAP 2010 apparatus between 0.1 and 0.995 mmHg with a homemade cell that allows analysing the complete monolith. Before analysis the monoliths were degassed for 2 h at 150 °C in vacuum. Pore size distribution was calculated using the BJH method.

Scanning electron microscopy (SEM) was carried out in a JEOL 5400 microscope. For cross sections analysis, the monoliths were previously coated with Pt in a Sputter Coater Telstar Emitech K-550 and then electrolitically coated with Ni to protect the layers during grounding and polishing. The line analysis and the mapping micrographs were obtained in a Hitachi S4800 SEM-FEG high-resolution microscope (1–3 nm) coupled to EDX Bruker X Flash Detector 4010 (133 eV resolution).

The adherence of the catalytic layer to the substrate was evaluated using an ultrasonic method previously described [26]. The adherence is defined as the ratio of retained amount of the catalytic layer after ultrasonic test and the amount of the deposited catalytic layer, expressed as percentage.

Roughness of pre-treated monoliths was measured with a Mitutoyo SJ-201P surface roughness tester.

In-depth compositional analysis of both the oxide and catalytic layers were determined by glow discharge optical emission spectroscopy (GD-OES) experiments using a LECO GDS 750A spectrometer. The GD-OES analyses were performed with a Grimm lamp in the DC mode at 700 V using a constant power of 14 W. A 4 mm area was analysed ensuring average macroscopic information of the analysed layers. Our system allows the analysis of up to 43 different elements from the periodic table, although, regrettably it does not allow that of gold.

The amount of alumina generated after anodisation per square meter of the aluminium sheets (g $Al_2O_3\ m_{Al}^{-2}$) was calculated from the amount of Al_2O_3 dissolved after 45 min in a solution composed by 35 ml of phosphoric acid (85 % Probus), 20 g of chromic acid (Panreac) and 1000 ml of distilled water, at 100 °C.

The gold loading in the deposited catalysts was quantified by inductively coupled plasma optical emission spectroscopy (ICP-OES) by measuring the gold content of the colloids before and after the deposition procedure in an ICP Perkin Elmer Optima 3000DV spectrometer.

Activity measurements

The catalytic oxidation of CO was performed in a conventional continuous flow U-shaped glass reactor working at atmospheric pressure. The composition of the inlet and outlet gases was analysed with a Balzers Omnistar Benchtop mass spectrometer. The light-off curves for CO oxidation (300 °C, $5\ °C\ min^{-1}$) were obtained with a gas mixture containing 3.4 % CO and 21 % O_2 balanced He (flow rate of $42\ ml.min^{-1}$). Blank reaction with an empty reactor showed no activity under these conditions. The catalytic devices were previously activated at 300 °C for 60 min in synthetic air and then stabilized at room temperature before the light-off curved started. Catalytic tests using powders catalysts were carried out in the same experimental conditions with 100 mg of solid diluted in 6 cm^3 of crushed glass beads (~200–400 μm) in order to maintain the residence time.

Results and discussion

Characterization of the metallic supports

XRD of the bare Fecralloy shows the characteristic peaks of a martensitic structure. After thermal pre-treatment, diffractions

due to corundum (α-Al$_2$O$_3$) phase appear (Fig. 1S—supplementary info). The alumina layer generated increases the roughness from 0.9 μm for bare metallic surface to 2.7 μm. The BET surface area of the whole pre-treated monolith is lower than 1 m^2. From the SEM analyses of the cross section (Fig. 1a), the thickness of the oxide layer is ≈3 μm, in good agreement with that estimated from GD-OES measurements (3.8 μm) (Fig. 1b). Besides alumina, GD-OES analysis also evidences the diffusion of silicon and, to a lesser extent, iron from the metal substrate to the oxide layer.

After anodisation, only XRD peaks of bare metal aluminium are detected, pointing to the amorphous character of the alumina layer produced (Fig. 1S—supplementary info). This layer has a singular cracked morphology (Fig. 2S—supplementary info), increasing the roughness of the surface from 0.7 to 4.5 μm. Also, its porous character is evidenced from the textual analysis, giving a BET surface area of 31 m^2 monolith^{-1}. GD-OES analysis (Fig. 1d) detects a surface enrichment in silicon, iron and titanium in the whole alumina layer. The thickness of this alumina layer, determined both by SEM and GD-OES, is ≈30 μm (Fig. 1c).

Characterization of the coated monoliths

Figure 3S (supplementary info) shows images of the used colloids and the prepared Fecralloy monoliths. While ceria colloid presents a yellowish colour, characteristic of cerium oxide, gold colloids have purple colours associated to the nanometric size of gold particles [27]. Differences in gold concentration could be responsible of the different purple tonalities observed for 0.1 and 1 % Au/CeO$_2$ colloids. Monoliths show homogeneous coatings where the colours of the colloids are maintained. In the Fecralloy monoliths as well as in anodised aluminium ones, the successful deposition of the catalytic layer was confirmed by SEM-EDX, being the adherence excellent whatever the catalyst deposited (≈99 % of the coating is retained after ultrasonic test).

The morphology of the catalytic coating was determined by the former morphology of the oxide layer generated in the pre-treatment. The particles of catalyst are inserted on the irregularities of such oxide layer, following the irregular branches and cracked structure of the anodised aluminium and the whiskers of α-Al$_2$O$_3$ in Fecralloy. The presence of gold does not alter the morphology of the layers, with the gold loading being determined by ICP-OES 0.88±0.03 wt.% and 0.124±0.049 wt.%, quite close to the target values of 1.0 wt.% and 0.1 wt.% respectively.

The deposition of CeO$_2$ on the metallic substrates was also proved by the observation of the characteristic X-ray diffraction peaks of cerianite phase (JCPDS=34-0394) in every monolithic device together with those of the corresponding substrate (Fig. 1S—supplementary info). The crystallite size of CeO$_2$, determined from the Scherrer equation was 5–6 nm, very similar to that of the powder catalyst [12], and it is preserved after gold introduction. Only for the catalyst loaded with 1%Au, an additional diffraction peak at $2\theta=38.1°$, due to the (200) plane of metallic gold (JCPDS=4-0784), was detected (Fig. 1S—supplementary info). From that diffraction,


Fig. 1 **a**, **c** Mirror-polished cross section and **b**, **d** GD-OES of pre-treated Fecralloy (*top*) and aluminium (*bottom*) monoliths
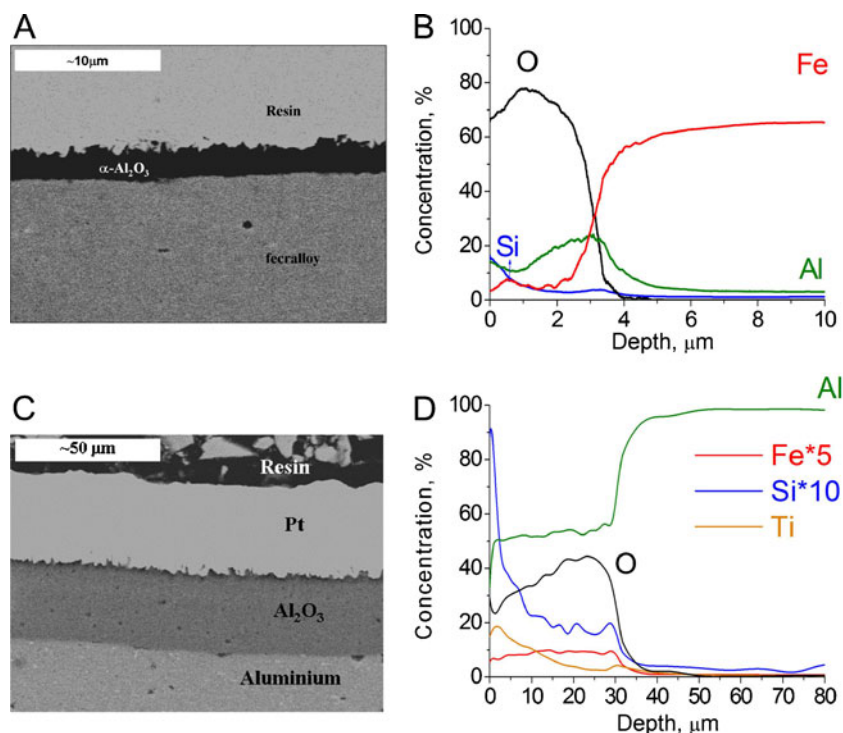
the average crystallite size of gold was calculated to be close to 20 nm, whatever the metallic monolith used. In good agreement, TEM and SEM observations (Fig. 2) reveal a good distribution of gold particles throughout the CeO_2 layer, their size ranging from 4 to 20 nm. Similar size and distribution of gold were reported for the AISI 304 monolithic catalysts prepared by the same method [12]. The existence of smaller gold particles cannot be overruled due to the lack of contrast between gold and ceria particles.

GD-OES allows estimating the in-depth composition and thickness of the coated catalytic layer. For Fecralloy monoliths, the thickness of the oxide scale increases after catalysts deposition up to 4.5 μm and 5.8 μm for CeO_2 and Au/CeO_2, respectively (Fig. 3a and b). Similar behaviour was also observed for austenitic stainless steel monoliths [12]. Cerium penetrates deep in the alumina layer reaching the oxide–alloy interface, although cerium concentration was higher in the outermost part of the oxide layer. Simultaneously, the migration of Si from the base alloy to the catalytic surface was evidenced by GD-OES, being higher for the monolith without gold. A silicon-rich layer is normally produced in the alloy–scale interface of stainless steels. This layer penetrates into the boundaries of the alloy grains and acting as protective barrier [28]. This way, the surface layer is not only composed of CeO_2 or Au/CeO_2, but also Si, Fe and aluminium oxide constitute the catalytic layer. Moreover, diffusion of chromium cations from the metallic substrate to the catalysts–substrate interface was detected by SEM-EDX in the case of the Fecralloy monolith coated with bare CeO_2 (Figs. 4 and 5). This chromium diffusion is not so evident in the samples with gold, pointing out the key role of the catalysts composition in the migration or not of elements. Unfortunately, a good profile for gold distribution was not obtained by SEM-EDX due to the low percentage of gold in the samples.

Figure 3c and d shows the GD-OES for CeO_2/aluminium monoliths. The alumina thickness generated after anodisation (≈30 μm) is preserved after catalyst deposition, probably because ceria penetrates the empty space between the cracks (following their irregularities) until the metallic interface and
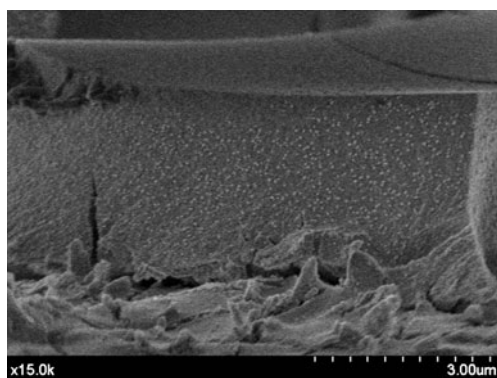
Fig. 2 Cross section of 1%Au/CeO_2/Fecralloy monolith

it never covers completely the alumina layer. The SEM-EDX study agrees with this explanation, since cerium is detected always associated with aluminium (Fig. 4).

Considering the migration of Si, Ti and Fe from the base alloy to the alumina layer observed in Fig. 3c, the final catalytic layer on CeO_2/aluminium monoliths is mainly composed of Al, Ce, Si, Ti and Fe. For Au/CeO_2/aluminium monoliths, the GD-OES profile (Fig. 3d) is quite similar to the profile with only ceria (Fig. 3c), the main difference being the small increment in the thickness of the oxide layer, up to 35 μm.

Thereby, GD-OES confirms that deposited cerium is not confined at the surface, penetrating through the oxide scale and reaching the substrate alloy in both metallic monoliths. The migration of cerium deposited on top of stainless steels to the alloy/scale interface has been widely demonstrated to occur independently of the way in which cerium were deposited: pyrolysis of aerosols, ion implantation or immersion in cerium nitrate solutions [29, 30]. Besides this, our SEM-EDX and GD-OES results show that the diffusion of several cations from the oxide scale of the metallic alloy to the catalytic layer also occurs. The qualitative (which cations) and quantitative (how much) metal migrations are related not only with the metallic substrate but also with the nature and composition of the catalyst deposited, resulting in different formulations and in-depth compositional profile of the catalytic layer. In this way, as remarked above, the thickness of the oxide scale is larger when the catalyst coating contains gold and, in the case of Fecralloy substrate, the presence of this metal could inhibit the chromium diffusion observed when only CeO_2 was deposited. This modification of the composition and distribution of the oxide scale with respect to the uncoated was previously pointed out for AISI 304 monoliths. In this case, the diffusion of Mn, Si, Cr and mainly Fe towards the catalytic layer was observed [12].

N_2 adsorption–desorption isotherms for coated monoliths correspond to typical mesoporous materials with complex pores structures made up of interconnected networks of pores of different size and shapes. The main textural parameters of the monoliths are summarized in Table 2.

After CeO_2 coating on Fecralloy monolith, the surface area and pore volume increase, reaching similar values to those obtained for AISI 304 monoliths. These surface areas are also in agreement with the S_{BET} value of CeO_2 powder catalyst. However, the pore volume of powder CeO_2 is lower than those measured for the coated monoliths, suggesting changes induced by the morphology/roughness of the washcoated metallic substrate. After gold insertion, a small expansion of the mesoporous structure was visible, simultaneously with an increase in the surface areas values. Whatever the stainless steel substrate used, the increments in both textural parameters were higher for 0.1 wt.%. Au catalysts than for 1 wt.%. Au ones. This behaviour could be linked to the different changes that the metallic alloy suffers in contact with the catalysts used. While 1 % Au could inhibit the migration of certain

Fig. 3 GD-OES of Fecralloy (*top*) and aluminium monolith (*bottom*) with **a, c** CeO_2 and **b, d** 1%Au/CeO_2 deposited
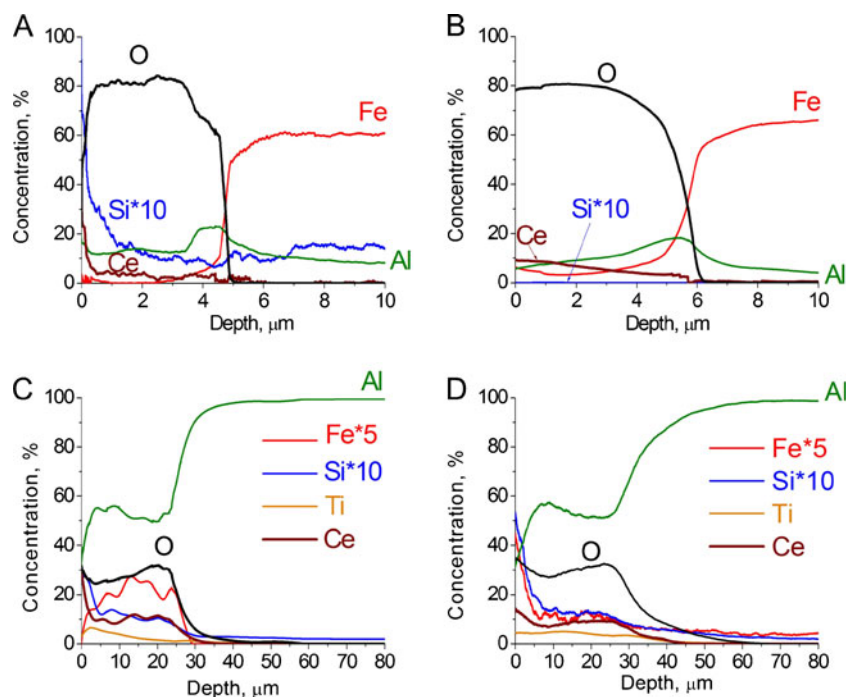
elements from the Fecralloy to the catalytic layer, a smaller gold concentration (0.1 %) is possibly not enough to prevent this migration.

Because of the high surface area of the alumina layer under the catalyst coating, textural properties for aluminium monoliths are different than for the stainless steels ones. CeO_2 anodised aluminium monolith presents the highest surface areas, decreasing these values when gold contents increases.

The textural properties of the powder gold catalysts show a different behaviour than that described for the washcoated monoliths. The 0.1 wt.%. Au sample has the same surface area and pore volume than the bare ceria support, while the addition of 1 % Au increases those values. This result demonstrates the influence of (1) the metallic substrate and (2) the gold content on the textural properties of the catalyst deposited on the monoliths.

Catalytic oxidation of CO

The pre-treated monoliths (without catalyst) show very low activities for CO oxidation, which depends on the metallic substrate used. AISI 304 stainless steel monolith [12] did not show any activity at temperatures below 300 °C, being the CO conversion at 500 °C lower than 5 %. Anodised aluminium monolith reached a CO conversion of 19 % at 500 °C. Finally, Fecralloy monolith showed the highest activity, 47 % CO conversion at 500 °C.

Table 3 shows the T_{50} and T_{80} values (temperatures to achieve 50 and 80 % of CO conversion) from the CO light-off curves of the prepared monoliths and the powder catalysts (Fig. 6). The most important differences in the shape of the

light-off curves are observed for CeO_2 catalyst devices (Fig. 6a), pointing out the different rate controlling regimes [31]. A detailed study of the controlling regimes needs more kinetic data that are out of the scope of this work. However, the differences in activity between powders and monoliths can be also addressed to the positive influence of the presence in the ceria layer of the elements coming from the substrate, as previously suggested for similar monolithic devices [12, 16, 32] and ceramic foams prepared from stainless steels wastes [21, 24] where the migration of metal cations, mainly Mn, Cr and Fe ones, were evidenced. In the present case, the simultaneous coexistence with the CeO_2 layer of elements like Si, Ti, Fe and Al, for anodised aluminium, and Si, Fe and Cr, for Fecralloy monoliths, could improve the activity response towards CO oxidation, since mixed oxides based on them (Fe_2O_3, TiO_2, CrO_x, CeO_2, etc.) have shown to be active catalysts and good supports in CO oxidation reactions [33–38]. This improvement is more significant for CeO_2/ Fecralloy monolith at low temperatures, reaching 50 % of conversion at 194 °C. The different shape of the light-off curves could be also related to changes in the chemical and/ or electronic structure adopted by the elements migrated and their interaction with the catalytic layer.

As expected, 0.1 % gold catalysts present an enhanced catalytic activity for CO oxidation (Fig. 6b). The equal or higher activity of the monoliths compared to that of the powder sample evidences, again, the positive role of the metal cations coming from the substrate, which is not so strange since it is well known that the catalytic activity of gold in oxidation reactions is strongly influenced by the doping with small quantities of transition metals or by the use of reducible

Fig. 4 Line analysis (*right*) of cross sections (*left*) of CeO$_2$ and 1%Au/CeO$_2$ deposited on Fecralloy and aluminium
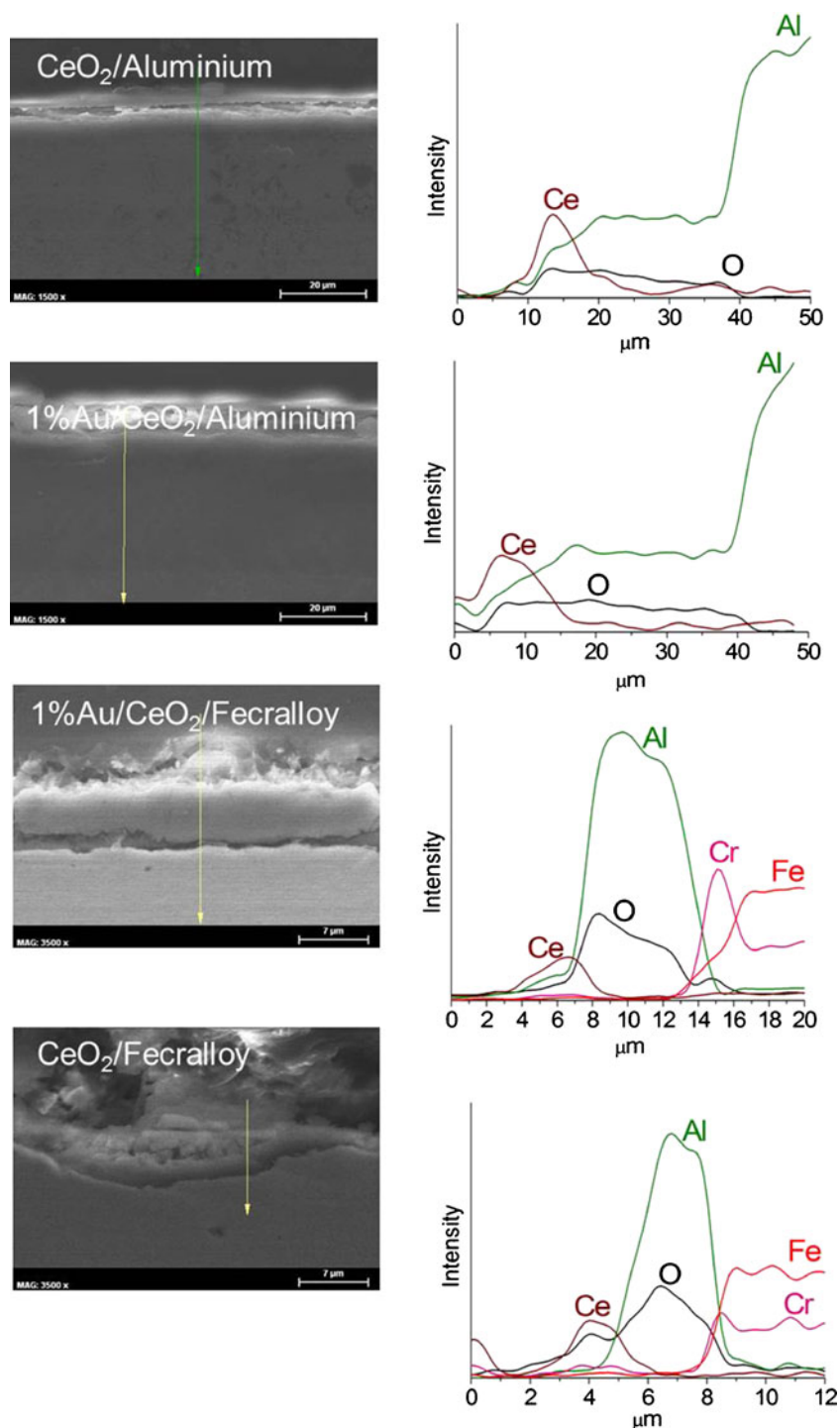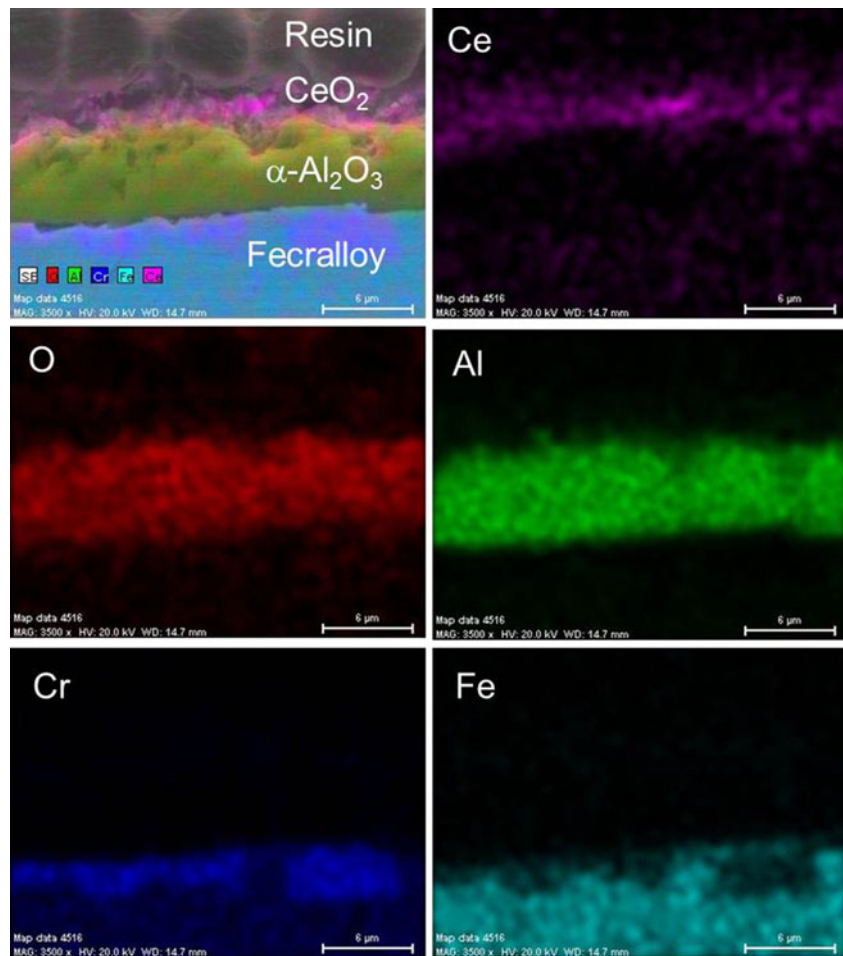

transition metal oxides as supports [39]. In this sense, it has been reported that the presence of metallic cations with active redox couples, such as Fe or Ti, and Ce, modifies the gold surface dynamics resulting in different Au particle sizes that could affect the catalytic behaviour of the catalyst [23]. On the other hand, all light-off curves are similar in shape, pointing out that the activity response should be mostly associated to the gold centres that should be similar in all catalysts. However, the

role of the elements coming from the substrate should also be taken account to explain the differences in activity.

Among the monolithic devices prepared with 0.1 % Au/ CeO$_2$ catalysts, a different sequence of activity is obtained as a function of the nature of the substrate with respect to that observed for the ceria-coated monoliths (Fig. 6a). The most active is that prepared on Fecralloy which has a CO conversion of 80 % at 146 °C. Anodised aluminium monolith is the

Fig. 5 Mapping of cross section of CeO$_2$/Fecralloy

second more active; meanwhile, the activity of the AISI 304 monolith is comparable to that of the powder catalyst. This observation must be related with the different qualitative and

Table 2 Textural properties of coating monoliths with CeO$_2$ and Au/CeO$_2$. Comparison with the powder catalysts

Monoliths	Catalysts	Surface area (m^2 catalytic device^{-1})	Pore volume (cm^3 monolith^{-1})	Average pore size (Å)
AISI 304[a]	CeO$_2$	10	0.014	41
	0.1%Au/CeO$_2$	15	0.014	41
	1%Au/CeO$_2$	13	0.011	53
Fecralloy	CeO$_2$	10	0.012	35
	0.1%Au/CeO$_2$	18	0.014	35
	1%Au/CeO$_2$	11	0.008	35
Anodised aluminium	CeO$_2$	32	0.045	148
	0.1%Au/CeO$_2$	28	0.056	147
	1%Au/CeO$_2$	24	0.052	148
Powders[a,b]	CeO$_2$	12	0.004	27
	0.1%Au/CeO$_2$	12	0.004	28
	1%Au/CeO$_2$	13	0.005	29

[a] Results for CeO$_2$/AISI 304 and 1%Au/CeO$_2$/monoliths and powder of CeO$_2$ and 1%Au/CeO$_2$ were obtained from reference [12]

[b] Results of surface area and pore volume calculated for 100 mg of catalyst (weight of catalyst used in every catalytic test)

Table 3 Catalytic activity of the monolithic devices

Monoliths	Catalysts	T (°C)	
		50 %	80 %
AISI 304[(a)]	CeO$_2$	209	232
	0.1%Au/CeO$_2$	168	190
	1%Au/CeO$_2$	83	92
Fecralloy	CeO$_2$	194	247
	0.1%Au/CeO$_2$	117	146
	1%Au/CeO$_2$	89	100
Aluminium	CeO$_2$	213	249
	0.1%Au/CeO$_2$	150	179
	1%Au/CeO$_2$	90	100
Powder catalyst	CeO$_2$	300	>500
	0.1%Au/CeO$_2$	137	188
	1%Au/CeO$_2$	86	103

[a] Results for AISI 304 monoliths and powder catalyst were obtained from Ref. [12]

Fig. 6 Conversion of CO with CeO$_2$ and Au/CeO$_2$ deposited on (*open upright triangle*) Fecralloy and (*filled star*) aluminium monoliths. Comparison with coated (*filled circle*) AISI 304 monoliths and (*plus sign*) powder catalysts [12]
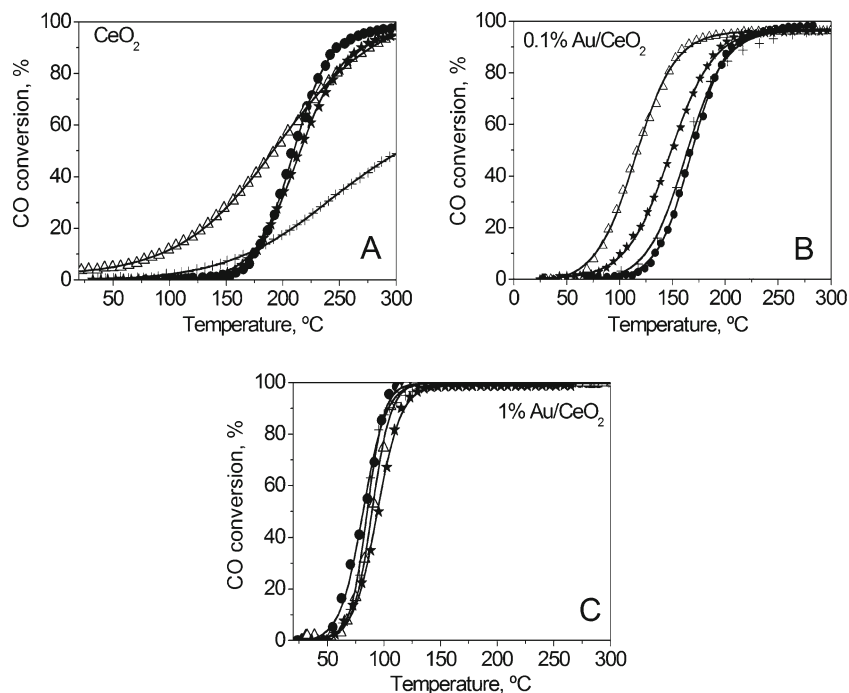
quantitative migration of elements when gold is present demonstrated by GD-OES and SEM studies, for instance, the minimised migration of chromium species in the case of Fecralloy substrate. In this regard, gold particles can nucleate on surface oxygen vacancies of ceria [15, 40] and therefore might migrate together with cerium to the alloy/scale interface, modifying the composition of the alloy. In fact, the migration of gold could induce redox reactions at the catalysts–substrate interface with other transition metals having redox pairs (Au^{n+}/Au^0, Ce^{4+}/Ce^{3+}, Fe^{3+}/Fe^{2+}, etc.) thus favouring the substrate oxidation and resulting in an increment of the thickness of the oxide scale, as observed by GD-OES results.

For the monoliths with 1 % Au/CeO$_2$, a full CO conversion is achieved at lower temperatures, obtaining similar activities and light-off shapes whatever the substrate used, and also comparable to that of the powder catalyst (Fig. 6c). It is clear that in this case, the CO oxidation properties of the devices should be ascribed essentially to the catalysts deposited in terms on gold available centres, and the differences induced in the catalysts formulation by the cations diffusion cause negligible modification of the oxidation capabilities of the system, at least in the reaction conditions tested. The good catalytic response of the 1%Au/CeO$_2$ catalysts avoid a clearer observation of the small differences produced associated to changes in the composition and or structure of the catalytic layer as compared with those of the powder sample.

On the other hand, the diffusion of elements could continue during the reaction. It is evident that if the sole interaction between the catalysts and the oxide scale of the substrate during the deposition step favours the migrations of cations in both directions despite the mild conditions in which such

process was carried out, the more aggressive conditions applied in the catalytic test probably reinforce such cationic diffusion. In fact, catalytic processes implying reaction atmospheres with high carbon activities attack metallic surfaces favouring carburization and metal dusting and resulting in extreme corrosion of the alloy [41]. Evidently, the extension of such degradation depends on the atmosphere composition and reaction conditions (temperature, time, pressure), and also of the metallic substrate and the structure and properties of the catalytic layer deposited. The initiation of damage is influenced by the microstructure, stress state and composition of the alloy, and the metal dusting process is enhanced at surface stress points and defects. The oxide scale can act as protector of the alloy degradation, but its effectiveness in inhibiting the onset of damage is lost in the presence of impurities and specimens able to catalyse carbon deposition [41] as occurs in CO oxidation conditions. To exemplify this, Figure 4S (supplementary info) shows the GD-OES results obtained for Fecralloy monoliths with CeO$_2$ catalysts. From that figure is evident that the Fe and Si migration from the alloy to the catalytic layer has continued during the catalytic test.

A more detailed study of the implications of such modifications in the catalytic active site (gold oxidation state, particle size, gold dispersion, redox properties, etc.) is actually under realisation.

Conclusions

In the present study, it was proved that the migrations of elements from the catalytic layer to the pre-treated metallic

substrate and conversely from the pre-treated metallic substrate to the catalytic layer occur after deposition of the catalysts on Fecralloy and anodised aluminium monoliths. In our case, the diffusion of cerium from the catalysts through the whole oxide scale, reaching the alloy/oxide scale interface, is observed. Beside this, Fe, Cr, Si and/or Ti from the metallic alloys were detected in the catalytic layer. The nature of the metallic substrate determines the nature and extension of the alteration in the catalytic coating composition. For Fecralloy-based monoliths, Si, Cr and Fe cations manage to arrive to the catalyst, while Ti, Si and Fe migrations occurs for anodised aluminium ones.

These alterations are also depending on the catalyst composition. Gold inhibits the migration of chromium in Fecralloy monoliths that was observed when only CeO_2 was deposited. This behaviour could explain the differences showed in the textural properties of 0.1 % Au catalysts with respect to 1 % Au.

As a consequence of these modifications, the composition, formulation and structure of the catalytic coating are altered and the catalytic performances of the structured device are compromised. The differences in the CO oxidation capabilities among the monolithic catalysts and with the powder ones are evident, especially in the lower active systems.

The evolution of the catalysts alteration continues during the catalytic reaction being a function of the atmosphere and reaction conditions used.

All these findings must be taken into account when preparing structured catalysts, especially on metallic surfaces, to be applied in environmental reactions in which a precise catalytic formulation is required. A careful study of the possible catalyst–substrate modification is mandatory in order to understand the different catalytic behaviours of the dispositive with respect to that of the powder catalysts.

References

1. Ávila P, Montes M, Miró EE (2005) Monolithic reactors for environmental applications: a review on preparation Technologies. Chem Eng J 109:11–36
2. Tronconi E, Groppi G (2000) A study on the thermal behavior of structured plate-type catalysts with metallic supports for gas/solid exothermic reactions. Chem Eng Sci 55:6021–6036
3. Martínez TLM, Sanz O, Domínguez MI, Centeno MA, Odriozola JA (2009) AISI 304 Austenitic stainless steels monoliths for catalytic applications. Chem Eng J 148:191–200
4. Schütze M (2000) In: Schütze M (ed) Corrosion and Environmental Degradation. vol. 1. Wiley, Weinheim
5. Stringer J (1989) The reactive element effect in high-temperature corrosion. Mater Sci Eng, A 120:129–137
6. Durán FG, Barbero BP, Cadús LE (2011) Preparation of MnO_x/AISI 304 austenitic stainless steel monoliths for catalytic combustion of ethyl acetate. Catal Lett 141:1786–1795
7. Milt VG, Ivanova S, Sanz O, Domínguez MI, Corrales A, Odriozola JA, Centeno MA (2013) Au/TiO_2 supported on ferritic stainless steel monoliths as CO oxidation catalysts. Appl Surf Sci 270:169–177
8. Chapman LR, Vigor CW, Watton JF (1982) Enhanced oxide whisker growth on peeled Al-containing stainless steel foils. US Patent 4331631
9. Frías DM, Nousir S, Barrio I, Montes M, Martínez TLM, Centeno MA, Odriozola JA (2007) Nucleation and growth of manganese oxides on metallic surfaces as a tool to prepare metallic monoliths. Appl Catal A: General 325:205–212
10. Burgos N, Paulís M, Montes M (2003) Preparation of Al_2O_3/Al monoliths by anodisation of aluminium as structured catalytic supports. J Mater Chem 13:1458–1467
11. Sanz O, Martínez TLM, Echave FJ, Domínguez MI, Centeno MA, Odriozola JA, Montes M (2009) Aluminium anodisation for Au-CeO_2/Al_2O_3-Al monoliths preparation. Chem Eng J 151:324–332
12. Martínez TLM, Sanz O, Centeno MA, Odriozola JA (2010) AISI 304 austenitic stainless steel monoliths: modification of the oxidation layer and catalytic coatings after deposition and its catalytic implications. Chem Eng J 162:1082–1090
13. Haruta M (1997) Size- and support-dependency in the catalysis of gold. Catal Today 36:153–166
14. Hutchings GJ (1996) Catalysis: a golden future. Gold Bull 29:123–129
15. Arzamendia G, Uriza I, Diégueza PM, Laguna OH, Hernández WY, Álvarez A, Centeno MA, Odriozola JA, Montes M, Gandía LM (2011) Selective CO removal over Au/CeFe and CeCu catalysts in microreactors studied through kinetic analysis and CFD simulations. Chem Eng J 167:588–596
16. Martinez TLM, Romero-Sarria F, Hernandez WY, Centeno MA, Odriozola JA (2012) Gold supported cryptomelane-type manganese dioxide OMS-2 nanomaterials deposited on AISI 304 stainless steels monoliths for CO oxidation. Appl Catal A: General 423–424:137–45
17. Moreau F, Bond GC, Hughes R, Moulijn JA, Makkee M, Krishna K, Silberova BAA (2007) Preparation of a monolith-supported Au/TiO_2 catalyst active for CO oxidation. Gold Bulletin 40(4):2191–94
18. Uriza I, Arzamendia G, Diégueza PM, Laguna OH, Centeno MA, Odriozola JA, Gandíaa LM (2013) Preferential oxidation of CO over Au/CuO_x–CeO_2 catalyst in microstructured reactors studied through CFD simulations. Catal Today. doi:10.1016/j.cattod.2013.04.023
19. Hammer N, Zarubova S, Kvande I, Chen D, Ronning M (2007) A novel internally heated Au/TiO_2 carbon-carbon composite structured reactor for low-temperature CO oxidation. Gold Bulletin 40(3):234–239
20. Martínez TLM, Frías DM, Centeno MA, Paúl A, Montes M, Odriozola JA (2008) Preparation of Au-CeO_2 and Au-Al_2O_3/AISI 304 austenitic stainless steel monoliths and their performance in the catalytic oxidation of CO. Chem Eng J 136:390–397
21. Dominguez MI, Sánchez M, Centeno MA, Montes M, Odriozola JA (2007) 2-Propanol oxidation over gold supported catalysts coated ceramic foams prepared from stainless steel wastes. JMol Catal A: Chem 277:145–154
22. Dominguez MI, Sanchez M, Centeno MA, Montes M, Odriozola JA (2006) CO oxidation over gold-supported catalysts-coated ceramic foams prepared from stainless steel wastes. Appl Catal A: General 302:96–103
23. Romero-Sarria F, Martínez TLM, Centeno MA, Odriozola JA (2007) Surface dynamics of Au/CeO_2 catalysts during CO oxidation. J Phys Chem C 111:14469–14475

24. Martínez TLM, Domínguez MI, Sanabria N, Hernández WY, Moreno S, Molina R, Odriozola JA, Centeno MA (2009) Deposition of Al-Fe pillared bentonites and gold supported Al-Fe pillared bentonites on metallic monoliths for catalytic oxidation reactions. Chem Engin J 151:324–332

25. Costello CK, Yang JH, Law HY, Wang Y, Lin JN, Marks LD, Kung MD, Kung HH (2003) On the potential role of hydroxyl groups in CO oxidation over Au/Al$_2$O$_3$. Appl Catal A: General 243:15–24

26. Zamaro JM, Ulla MA, Miró EE (2005) The effect of different slurry compositions and solvents upon the properties of ZSM5-washcoated cordierite honeycombs for the SCR of NOx with methane. Catal Today 107–108:86–93

27. Bond GC, Louis C, Thompson DT (2006) Catalysis by gold. Catalytic Science Series. Imperial College Press 6: 41

28. Paul A, Elmrabet S, Ager FJ, Odriozola JA, Respaldiza MA, da Silva MF, Soares JC (2002) Influence of preoxidation and annealing treatments on the isothermal oxidation in air at 1173 K of cerium-implanted EN-1.4301 stainless steel. Oxid Metals 57:33–51

29. Capitan MJ, Paul A, Pastol JL, Odriozola JA (1999) X-ray diffraction study of oxide scales formed at high temperatures on AISI 304 stainless steel after cerium deposition. Oxid Met 52:447–462

30. Paúl A, Elmrabet S, Ager FJ, Odriozola JA (2000) High temperature oxidation behaviour of EN-1.4301 stainless steel after surface Ce deposition by a modified CVD method. Surf Int Anal 30:176–180

31. Joshi SY, Harold MP, Balakotaiah V (2010) Overall mass transfer coefficients and controlling regimes in catalytic monoliths. Chem Eng Sci 65:1729–1747

32. Wolff IM, Iorio LE, Rumpf T, Scheers PVT, Potgieter JH (1998) Oxidation and corrosion behaviour of Fe–Cr and Fe–Cr–Al alloys with minor alloying additions. Mater Sci Eng, A 241:264–276

33. Laguna OH, Centeno MA, Arzamendi G, Gandía LM, Romero-Sarria F, Odriozola JA (2010) Iron-modified ceria and Au/ceria catalysts for total and preferential oxidation of CO (TOX and PROX). Catal Today 157:155–159

34. Schubert MM, Venugopal A, Kahlich MJ, Plzak V, Behm RJ (2001) Influence of H$_2$O and CO$_2$ on the selective CO oxidation in H$_2$-rich gases over Au/α-Fe$_2$O. J Catal 197:113–122

35. Boccuzzi F, Chiorino A, Manzoli M, Andreeva D, Tabakova T (1999) FTIR study of the low-temperature water-gas shift reaction on Au/Fe$_2$O$_3$ and Au/TiO$_2$ catalysts. J Catal 188:176–185

36. Park PW, Ledford JS (1998) Characterization and CO oxidation activity of Cu/Cr/Al$_2$O$_3$ catalysts. Ind Eng Chem Res 37:887–893

37. Yuzefovich GE, Gura RP (1977) Catalytic oxidation of carbon monoxide by oxygen and nitrogen oxides on a copper-chromium oxide catalyst. Reac Kinet Catal Lett 6:175–179

38. Laine J, Ferrer Z, Labady M (1988) Structure and activity of chromium-promoted Raney copper catalysts for carbon monoxide oxidation. Appl Catal 44:11–22

39. Schubert MM, Hackenberg S, Van Veen AC, Muhler M, Plzak V, Behm RJ (2001) CO oxidation over supported gold catalysts—"inert" and "active" support materials and their role for the oxygen supply during reaction. J Catal 197:113–122

40. Penkova A, Chakarova K, Laguna OH, Hadjiivanov K, Romero-Sarria F, Centeno MA, Odriozola JA (2009) Redox chemistry of gold in a Au/FeO$_x$/CeO$_2$ CO oxidation catalyst. Catal Commun 10:1196–1202

41. Di GF, Bernstein JR, Al-Qhatani MM, Liu Z, Jordan MP, Richardson JA, Stott FH (2003) Study of the metal dusting behaviour of high-temperature alloys. Mat Corrosion 54:854–859